Deposition in porous media and clogging on the field scale

E. A. Borisova and P. M. Adler
IPGP, 4, Place Jussieu, 75252-Paris-Cedex 05, France
(Received 10 July 2004; revised manuscript received 25 August 2004; published 14 January 2005)

Deposition is modeled as a first order reaction on the Darcy scale for porous media which are statistically homogeneous. An elementary analytical solution is derived. A parametric study was done with a three-dimensional code which is briefly described and checked in media where the solution is known. The role of the parameters, including the artificial ones, is discussed with an illustrative example. When the Damköhler number is small, deposition causes smooth changes to the porosity field; the evolution of porosity is well described by the analytical solution. Very different results are obtained for large Damköhler numbers. The influence of the correlation of the initial porosity field is studied.

DOI: 10.1103/PhysRevE.71.016311 PACS number(s): 47.70.Fw, 47.55.Mh

I. INTRODUCTION

Deposition in porous media is a process of high practical and fundamental interest, since this problem arises in various branches of industry, particularly in chemical, civil, and petroleum engineering. For instance, the deposition at the solid surface of a reservoir may considerably diminish the oil production. Other standard applications include water treatment and environmental studies of transport of chemical contaminants. A recent application is the reduction of the release rate of carbon dioxide to the atmosphere by mineral trapping in deep permeable geologic formations (Xu *et al.* [1]).

The topic of changes in hydrologic properties due to chemical reactions has recently been reviewed by Saripalli *et al.* [2]. Most of the understanding of the reactive transport has been obtained on the pore scale. On this scale, the term deposition can be used in different meanings, referring either to the solute precipitation on the fluid-solid interface, to the trapping of fine particles at pore throats, or to ion exchange, etc. These processes cause morphological changes of the pore space and can lead to porosity and permeability decreases.

Sahimi *et al.* [3] reviewed models of fluid-solid interactions in porous media. Shapiro and Brenner [4] studied dispersion of a chemically reactive solute in spatially periodic porous media; however, the geometry of the medium was assumed to be fixed. The precipitation of a reactive solute at the fluid-solid interface in porous media and the subsequent morphological changes of the pore space were discussed by Sallès *et al.* [5]. Matthews *et al.* [6] simulated the subtle changes in void space dimensions which occur during the artificial deposition of small amounts of illite and kaolinite within sandstones. They compared the mercury intrusion curves of an untreated plug of sandstone and of a similar plug in which the deposit has been precipitated.

Deposition in fracture networks is not often addressed in the literature. Mourzenko *et al.* [7] and Békri *et al.* [8] studied deposition in a single fracture. They considered deterministic and random fractures and the changes in fracture morphology were taken into account. Deposition in fracture networks is lacking at the moment and the properties have not been upscaled yet.

Chang and Civan [9] developed a model which can satisfactorily simulate the permeability alteration mechanisms caused by hydrodynamic, physico-chemical and chemical interactions between fluids and reservoir rocks. Xu *et al.* [1] developed a reactive fluid flow and geochemical transport numerical model for evaluating long-term CO_2 disposal in deep geologic formations. This study makes use of an existing nonisothermal reactive geochemical transport model TOUGHREACT [10]. It was applied to a one-dimensional (1D) radial flow which schematizes flow around a well. No change in the transport properties was taken into account though it is possible.

As a rule, the results of the pore scale simulations are compared to the experimental measurements on the core samples which are supposed to be homogeneous. Reservoir simulations are applied to fields extending from several meters to kilometers. In this case, the geological structure of the reservoir is taken into account by means of the macroscopic parameters which vary in space and time. Liu *et al.* [11] describe a two-dimensional geochemical simulator, CIRF.A, and its application to matrix acidizing analysis and design. The effects of diagenesis on the properties of sandstone reservoirs were addressed by Le Gallo *et al.* [12]. They developed a three-dimensional, two phase, reaction-transport simulator named DIAPHORE which couples kinetically controlled dissolution and precipitation of minerals with equilibrium reactions of chemical species in the water phase. In reservoir simulations, the ability of the core-scale data to represent the macroscopic properties of discretization blocks is not obvious since in real rocks the macroscopic parameters can vary within a block. This variability must be taken into account and the validity of the permeability-porosity relationships must be verified.

An appropriate averaging technique requires an investigation of the deposition phenomenon on the intermediate scale which corresponds to the discretization block. The major purpose of this work is to implement this technique numerically and to study deposition and the subsequent changes of the macroscopic properties in statistically homogeneous porous media. To describe such media, a discrete model was used with uniform porous subdomains possessing various physical properties. Statistically homogeneous materials are viewed as being spatially periodic, i.e., as composed of identical heterogeneous cells.

 ©2005 The American Physical Society

Section II provides a general overview on the deposition process of a chemical solute and on subsequent changes of the macroscopic properties of the porous medium. We consider a three-dimensional transport of the solute in the presence of a first order irreversible reaction at a fluid/rock surface. The coupling between the changes of macroscopic parameters and the reactive transport uses a quasisteady hypothesis. In Sec. IV, this assumption is justified and the corresponding algorithm is described. The flow and transport equations are solved numerically by means of a finite volume technique; porosity changes are governed by a balance equation. A brief discussion on the code performance is given at the end of the section.

Section III provides the necessary constitutive equations derived from previous studies on the local scale such as the relation between porosity and permeability, the local dispersion tensor and the local deposition rate. It gives also the initial porosity fields whose evolution will be studied. The numerical algorithm is detailed in Sec. IV. An elementary solution for the porosity evolution is derived; it will be systematically compared to the numerical results. The main dimensionless quantities are defined in this section.

Section V presents the numerical results. Preliminary verifications of the code on several configurations are detailed. Then, three realizations of statistically equivalent media are generated and very close results are obtained for them. The influence of the unit cell size was studied by comparing the results for various ratios of the correlation length and of the unit cell size. The influence of the discretization has been studied; it appears that the size of the elementary cube is small enough that the discretization does not influence the results. The influence of the Damköhler number is studied; two regimes are shown to exist for small and high Damköhler numbers. The main statistical parameters of the initial porosity field are also briefly addressed. Finally, the influence of the nature of the initial porosity field is studied. A few concluding remarks end this paper.

II. GOVERNING EQUATIONS

Let us start by a general presentation of the problem; initial configurations of the studied porous media are illustrated in Fig. 1. Consider some chemical solute contained in underground water. While flowing through the porous medium, the solute precipitates onto the solid surface of the medium. Fresh solute is supposed to be brought so that the mean volumetric liquid concentration remains constant all the time. Moreover, we assume that the macroscopic gradient of concentration is negligibly small. This may correspond to a physical situation where the region of interest is located sufficiently far away from injection/production wells. Deposition implies porosity, permeability and other macroscopic parameter changes. After a very long time, if fresh solute is constantly brought by the fluid, the permeability of the medium will tend towards zero.

A. Flow

The seepage velocity $\overline{\mathbf{v}}$ inside the porous domain is governed by the Darcy equation,

$$\overline{\mathbf{v}} = -\frac{\mathbf{K}}{\mu} \cdot \boldsymbol{\nabla} P, \tag{2.1}$$

where $\mathbf{K}$ is the permeability tensor, μ the fluid viscosity, and P the pressure.

The pressure field may be obtained by solving the continuity equation,

$$\boldsymbol{\nabla} \cdot \overline{\mathbf{v}} = 0. \tag{2.2}$$

A nonzero macroscopic pressure gradient is imposed along a given direction over the unit cell,

$$\overline{\boldsymbol{\nabla} P} = \text{const}. \tag{2.3}$$

This direction is arbitrarily chosen to be the x-axis. Note that due to the deposition process, the permeability tensor in (2.1) depends on time.

B. Convection-dispersion

On the macroscopic scale, the transport of a reactive solute is governed by a three-dimensional convection-dispersion equation with reaction

$$\frac{\partial C\varepsilon}{\partial t} + \boldsymbol{\nabla} \cdot (C\overline{\mathbf{v}}) = \boldsymbol{\nabla} \cdot (\overline{\mathbf{d}} \cdot \boldsymbol{\nabla} C) - R, \tag{2.4}$$

where C is the solute concentration, ε the porosity, $\overline{\mathbf{d}}$ the macroscopic dispersion tensor and R the reaction term. It is assumed that on the macroscopic scale, dispersion is Fickian and can be described by a dispersion tensor [13]. Moreover, $\overline{\mathbf{d}}$ depends on the local porosity and on the fluid velocity as it will be seen below.

C. Reaction and porosity changes

In the present work, an irreversible first order reaction is considered. Note that the reaction occurs at the solid-fluid interface on the pore scale. On the macroscopic scale, the heterogeneous reaction is expressed by means of a sink term R [14] which can be modeled as

$$R = \begin{cases} \gamma\varepsilon(C - C^*) & \text{if } C > C^*, \\ 0 & \text{if } C \leqslant C^*, \end{cases} \tag{2.5}$$

where C^* is the saturation concentration on the solid surface and γ the volumetric reaction rate. γ is an unknown function which depends on deposition on the pore scale. It will be given later.

Due to deposition, porosity decreases with time as described by the balance equation

$$f\frac{\partial}{\partial t}(1 - \varepsilon) = R, \tag{2.6}$$

where f is the solid fraction in the deposit [5]; for instance, for a random packing of monodisperse spheres, f is equal to 0.64.

It is generally assumed in this paper that the amount of precipitating solute is unlimited and that the porosity can

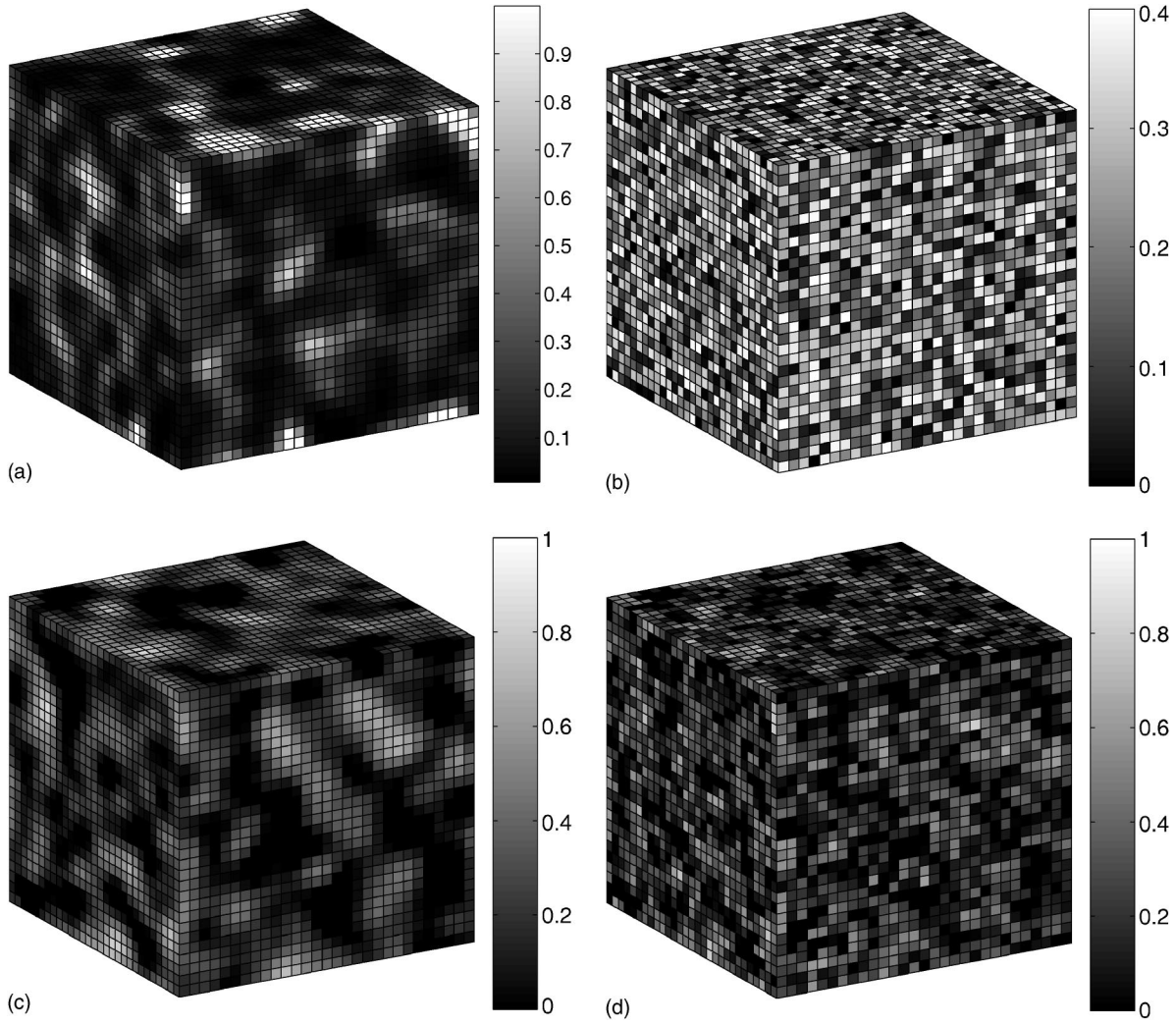

FIG. 1. Examples of initial porous media. Porosity is given by the grey scale (see the vertical bars). Examples are for (a) a lognormal porosity field with a Gaussian correlation function (which is studied at length in Sec. V A); (b) a uniformly distributed porosity field; (c) a Gaussian porosity field; (d) a self-affine porosity field. For the three cases (b), (c), and (d), $\langle \varepsilon_0 \rangle = 0.2$, $\sigma_0 = 0.2$, and $\lambda / L_c = 8/30$.

decrease until the porous medium is clogged. This hypothesis will be discussed at the end of Sec. V A 2.

D. Dimensionless formulation

In order to derive the dimensionless parameters which control the problem, the governing equations should be expressed in dimensionless form. Let us define the dimensionless variables

$$\mathbf{r}' = \frac{\mathbf{r}}{L}, \quad \overline{\mathbf{d}}' = \frac{\overline{\mathbf{d}}}{\gamma_0 L^2}, \quad t' = \gamma_0 t, \quad C' = \frac{C - C^*}{C_0 - C^*},$$

$$\mathbf{v}' = \frac{\mathbf{v}}{V^*}, \quad \gamma' = \frac{\gamma}{\gamma_0}, \quad f' = \frac{f}{C_0 - C^*}, \quad \nabla' = L \nabla, \tag{2.7}$$

where L, V^* are some characteristic values of length and velocity; it seems natural that L is chosen to be the field scale. Accordingly, γ_0 is a characteristic value of the reactivity γ; note that it has the dimension of the inverse of a time. The average liquid concentration C_0 is kept constant with time and it may be expressed as

$$C_0 = \frac{\int_\Omega C \varepsilon d^3\mathbf{r}}{\int_\Omega \varepsilon d^3\mathbf{r}}, \tag{2.8}$$

where Ω is the whole domain volume.

Let us define the Damköhler number by the standard relation

$$\mathrm{Da} = \frac{\gamma_0 L}{V^*}. \tag{2.9}$$

With the help of (2.7) and (2.9), (2.4) can be written as

$$\frac{\partial \varepsilon C'}{\partial t'} + \frac{1}{\mathrm{Da}} \nabla' \cdot (C' \overline{\mathbf{v}'}) - \nabla' \cdot (\overline{\mathbf{d}'} \cdot \nabla' C') = -\gamma' \varepsilon C'. \tag{2.10}$$

The Damköhler number compares the reaction rate to convection. Alternate choices are of course possible for the units and the dimensionless numbers.

III. THE CONSTITUTIVE EQUATIONS AND THE POROSITY FIELD

A. The constitutive equations

Constitutive parameters such as the permeability $\mathbf{K}$ and the macroscopic dispersion tensor $\overline{\mathbf{d}}$ depend on the pore geometry of the medium. Their determination is a local scale problem which involves the analysis of the microstructure of the porous medium. In this study, a simple model is used for $\mathbf{K}$,

$$\mathbf{K} = K_0 \mathbf{I} \varepsilon^{\eta}, \tag{3.1}$$

where K_0 is a characteristic permeability and $\mathbf{I}$ the unit tensor. The exponent η is generally taken equal to 4 [15–17].

The dispersion tensor can be approximated as a sum of the macroscopic diffusion tensor $\overline{\mathbf{d}}_0$ and of the tensor $\hat{\mathbf{d}}^*$ which depends on the local Péclet number,

$$\overline{\mathbf{d}} = \overline{\mathbf{d}}_0 + \varepsilon D_m \hat{\mathbf{d}}^*, \tag{3.2}$$

where D_m is the molecular fluid diffusion. The macroscopic diffusion coefficient will be written as

$$\overline{\mathbf{d}}_0 = D_m \mathbf{I} \varepsilon^2, \tag{3.3}$$

which corresponds to the relation obtained by Coelho *et al.* [17] for random packings of spheres in agreement with Archie's law with a cementation exponent equal to 2. In a coordinate system where the x-axis is parallel to the Darcy velocity $\overline{\mathbf{v}}$, the tensor $\hat{\mathbf{d}}^*$ has a diagonal form

$$\hat{\mathbf{d}}^* = \begin{pmatrix} d_{\parallel} & 0 & 0 \\ 0 & d_{\perp} & 0 \\ 0 & 0 & d_{\perp} \end{pmatrix}, \tag{3.4}$$

when the porous medium is locally isotropic; $d_{\parallel}$ is the longitudinal dispersion and $d_{\perp}$ the transversal dispersion. They can be estimated as power functions of the local Péclet number $\mathrm{Pe}_{\mathrm{loc}}$,

$$d_{\parallel} = \beta_{\parallel} \mathrm{Pe}_{\mathrm{loc}}^{\alpha_{\parallel}}, \quad d_{\perp} = \beta_{\perp} \mathrm{Pe}_{\mathrm{loc}}^{\alpha_{\perp}}. \tag{3.5}$$

The local Péclet number is defined as

$$\mathrm{Pe}_{\mathrm{loc}} = \frac{V^* l}{D_m}, \tag{3.6}$$

where l is some local characteristic length. l can be chosen equal to the correlation length of the pore space. In this work, l is taken equal to 0.5 mm. The molecular diffusion D_m of a reactive solute in water phase is of the order of 10^{-9} m.

The approximation of the results obtained by Coelho *et al.* [17] for random packings of spheres yields the following quantities. For $\mathrm{Pe}_{\mathrm{loc}} \in [0.1, 1]$, the values of the coefficients are of the order of

$$\beta_{\parallel} = 0.175, \quad \alpha_{\parallel} = 0.305, \quad \beta_{\perp} = 0.127, \quad \alpha_{\perp} = 0.159. \tag{3.7a}$$

For $\mathrm{Pe}_{\mathrm{loc}} \in [1, 10^5]$, they are of the order of

$$\beta_{\parallel} = 0.175, \quad \alpha_{\parallel} = 1.285, \quad \beta_{\perp} = 0.127, \quad \alpha_{\perp} = 0.80. \tag{3.7b}$$

Since (3.4) is valid in a local coordinate system, one must make coordinate changes depending on the velocity orientations at each point where the dispersion tensor is needed.

The last quantity of interest is the volumetric reaction rate γ (cf. Sec. II C). It can be estimated in a very crude way from the knowledge of the surface reaction rate constant k_p which does not depend on the morphology of the pore space. This can be done as follows. The hydraulic radius m is usually defined as the ratio of the fluid volume V_f to the pore surface area S_p,

$$m = \frac{V_f}{S_p}. \tag{3.8}$$

V_f and S_p are relative to a total volume V. The reaction term R is proportional to the pore surface area per unit volume

$$R = k_p \frac{S_p}{V} (C - C^*) = \gamma \varepsilon (C - C^*). \tag{3.9}$$

Hence, the effective volumetric reaction rate constant is

$$\gamma = \frac{k_p}{m}. \tag{3.10}$$

The hydraulic radius m decreases during the deposition process. It is difficult to predict the evolution of this parameter. There are several useful relations described in the literature for the hydraulic radius. Usually, m depends on the microscopic geometry of the medium. We suppose that locally the deposition process is limited by the surface reaction kinetics. In that case, a uniform deposition is expected [7]. Since the medium is supposed to be granular, the grains are coated by a uniform layer of deposited matter. For random packings of monodisperse spheres, m can be expressed as

$$m(t) = m_c \varepsilon(t)^{3/4}, \tag{3.11}$$

where m_c is some constant. This relation roughly describes the hydraulic radius variations for random packings of monodisperse spheres when the initial porosity is about 0.4. It was shown that the specific surface area of consolidated media is only slightly affected by a slow deposition process [7,12]. For small porosities, the hydraulic radius is taken to be constant. Note that the relations presented above are only meant to provide reasonable orders of magnitude.

Since, on the pore scale, the deposition process is assumed to be reaction-limited, it is useful to provide an expression for the relationship between the Damköhler numbers Da_p and Da on the pore scale and on the field scale, respectively. Da_p is expressed as

$$\mathrm{Da}_p = \frac{k_p}{v_p}, \tag{3.12}$$

where v_p is the local interstitial velocity. Thus, Da_p and Da are related by

$$\mathrm{Da} = \frac{L}{\langle m_0 \rangle} \frac{v_p}{V^*} \mathrm{Da}_p. \tag{3.13}$$

Since on the local scale deposition is assumed to be reaction-limited, one has

$$\mathrm{Da}_p \ll 1. \tag{3.14}$$

Hence, (3.13) shows that because of the length scale ratio, Da can be very large while Da_p is very small.

B. Description of the initial porosity field

The porosity field is generated numerically as a random correlated or noncorrelated field. Usually, local properties of the real porous media are described by lognormal distributions [20]. In this paper, uniform and Gaussian distributions were also used.

The uniform distribution corresponds to porosity values uniformly distributed on some interval, for example, between 0 and 0.4.

The probability density of the Gaussian distribution is expressed as

$$f(x) = \frac{1}{\sqrt{2\pi\sigma_G^2}} \exp\left(-\frac{1}{2} \frac{(x-\mu_G)^2}{\sigma_G^2} \right), \tag{3.15}$$

where μ_G is the mean and σ_G^2 the variance.

Another class of random distributions is the lognormal distribution. If y_G is a Gaussian random variable with mean μ_G and variance σ_G^2, the variable $y_{LN}=\exp(y_G)$ is lognormally distributed. Its mean and variance are given by

$$\mu_{LN} = \exp\left(\mu_G + \tfrac{1}{2}\sigma_G^2\right), \quad \sigma_{LN}^2 = \exp(2\mu_G + 2\sigma_G^2) - \mu_{LN}^2. \tag{3.16}$$

The spatial organization of the porosity field also needs to be defined. Two major types of structures can be easily implemented by means of the correlation function

$$C(\mathbf{u}) = \frac{\langle [\varepsilon(\mathbf{x}+\mathbf{u}) - \mu_\varepsilon][\varepsilon(\mathbf{x}) - \mu_\varepsilon] \rangle}{\langle (\varepsilon(\mathbf{x}) - \mu_\varepsilon)^2 \rangle}, \tag{3.17}$$

where $\mu_\varepsilon = \langle \varepsilon \rangle$.

The porosity field is said to be Gaussian when its correlation C is Gaussian,

$$C(\mathbf{u}) = \sigma_G^2 \exp\left[-\left(\frac{u_x}{\lambda_x}\right)^2 - \left(\frac{u_y}{\lambda_y}\right)^2 - \left(\frac{u_z}{\lambda_z}\right)^2 \right], \tag{3.18}$$

where λ_x, λ_y, λ_z are the correlation lengths along the x, y, and z directions, respectively. $\mathbf{u}$ is the shift with components (u_x, u_y, u_z). Let us denote by $\hat{C}(\mathbf{k})$ the Fourier transform of the correlation function $C(\mathbf{u})$. Self-affine porosity fields are defined by

$$\hat{C}(\mathbf{k}) \propto [1 + (\lambda_x k_x)^2 + (\lambda_y k_y)^2 + (\lambda_z k_z)^2]^{-H/2}, \tag{3.19}$$

where H is the Hurst exponent. The Gaussian correlated field is generated by means of the Fourier transform method which is described by Adler and Thovert [18].

The fields generated by these two correlations are very different and will be illustrated in Sec. V.

IV. PRELIMINARIES TO THE NUMERICAL STUDY

A. Numerical solution

The problem is solved in a parallelepipedic cell discretized into $N_{cx} \times N_{cy} \times N_{cz}$ elementary cubes. Each elementary cube has given porosity, diffusion, and permeability tensors. The continuity equation, the reactive transport equation, and the equation for porosity changes were discretized using a finite volume method. The pressure and concentrations are evaluated at the cube corners. The pressure field was obtained by using a box integration technique.

To solve the transport equations, one is usually interested in a shock-capturing numerical model, which does not produce spurious oscillations near discontinuities and yet remains stable. These properties are quite important for simulating convection-dispersion phenomena, especially for situations where convection is dominant. Therefore, our main effort was to reduce numerical dispersion. One possible way to achieve it is to apply an operator-splitting technique. The idea is to solve the convection part up to a certain time step δt and then to add the dispersive effects in a separate step. The second order flux limiting scheme was applied to solve the convection equation [19]. For this method, the best accuracy is obtained when the time step is chosen as large as the stability criterion for the convective part allows. Operator splitting has the advantage that the time step for the convection part may be optimized to reduce numerical dispersion. Then, the dispersive part may be solved implicitly or exlicitly. Here, the dispersion-reaction part was addressed by a classical explicit scheme. When the convective shift for δt is calculated, the dispersion equation is solved n times for time step $\delta t_s = \delta t / n$. Usually, convective transport is predominant in underground formations. Thus, the restrictions on the convection time step are more severe than that for dispersion and $n=1$.

The code was tested on several cases where the analytical solution is available. A special attention was put on checking the extreme situations, such as pure convection, convection-dispersion, diffusion-reaction, and convection-reaction. Usually, a good agreement between numerical results and analytical predictions is observed.

In Sec. II, the governing equations are introduced into the framework of a continuous description. To solve these equations numerically, a quasisteady hypothesis is assumed. The idea is the following. As long as the porosity changes are not significant, i.e., they do not exceed a value $\Delta\varepsilon_{\max}$ prescribed in advance, we suppose that the macroscopic parameters and local velocities do not change. Thus, the conservation equation for pressure is solved with constant parameters, i.e., for a fixed situation. Then, asymptotically the concentration field

is expected to decay exponentially with time, but uniformly in space [4]. This corresponds to

$$C'(\mathbf{r}',t') = \hat{C}'(\mathbf{r}')\exp(-Bt'), \tag{4.1}$$

where B is some decay rate.

Hence, when this exponential regime takes place, the following ratio over a constant time step $\delta t'$ becomes constant:

$$\frac{\int_\Omega C'(\mathbf{r}',t')d^3\mathbf{r}'}{\int_\Omega C'(\mathbf{r}',t'-\delta t')d^3\mathbf{r}'} = \exp(B\delta t'). \tag{4.2}$$

Thus, denote

$$\alpha(t') = \ln\left(\frac{\int_\Omega C'(\mathbf{r}',t')d^3\mathbf{r}'}{\int_\Omega C'(\mathbf{r}',t'-\delta t')d^3\mathbf{r}'}\right). \tag{4.3}$$

The convergence test consists in checking the absolute value of the time derivative of $\alpha(t')$. We assume that the time necessary to reach such a regime is very small compared to the deposition time. Hence, the transport equations are iterated until the concentration field reaches the exponential regime.

Then, the porosity changes can be easily obtained as functions of time by solving Eq. (2.6). Thus, it is possible to calculate the time τ during which the maximal porosity change $\Delta\varepsilon_i$ exceeds the prescribed threshold $\Delta\varepsilon_{\max}$ in any elementary cube i,

$$\tau = \{\delta t' : \varepsilon_i(t_0') - \varepsilon_i(t_0' + \delta t') \approx \Delta\varepsilon_{\max}\}. \tag{4.4}$$

The new values of the porosity field and of the other macroscopic parameters are calculated according to the amount of matter deposited during τ in each elementary cube. Then, the calculations are iterated with these new parameters.

The program is stopped when the macroscopic permeability of the porous medium is 10^3 times smaller than the initial one. Some additional comments on this point can be found at the end of Sec. V A 2. A schematic representation of the algorithm is given in Fig. 2.

Several assumptions used in this problem need to be confirmed by quantitative comparisons with experimental data, but to the best of our knowledge, no experimental work is available on this subject. Such a verification is especially necessary when the deposition rate is large, with rapid changes of the geometry of the pore space; in such a case, the concentration profile may never reach the exponential regime.

B. An elementary solution

An elementary solution can be derived from (2.6) when the concentration C' and the reactivity γ' are assumed to be constant. Obviously,

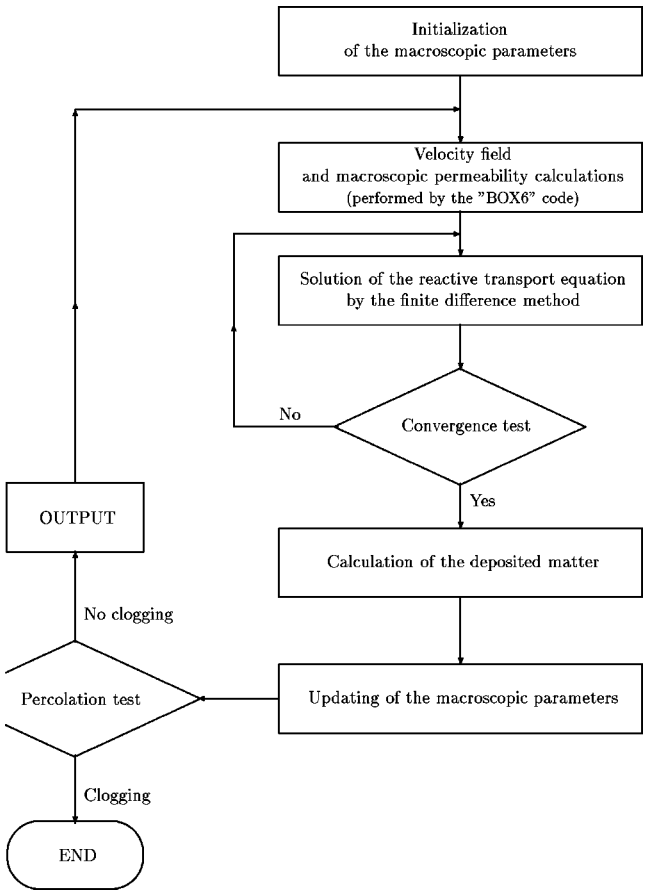

FIG. 2. Schematic representation of the algorithm.

$$\frac{\partial}{\partial t'}(1-\varepsilon) = \frac{\gamma'}{f'}\varepsilon C'. \tag{4.5}$$

Moreover, this relation can be averaged over the cell and it yields an exponential decay for the average porosity $\langle\varepsilon\rangle$,

$$\langle\varepsilon\rangle = \langle\varepsilon_0\rangle\exp\left(-t'\frac{\gamma'}{f'}C'\right). \tag{4.6}$$

This elementary solution will prove to be very useful.

C. Characteristic quantities, output quantities, and dimensionless parameters

The choice of the characteristic parameters is very important since they define the dimensionless parameters controlling the process. The characteristic length L is chosen equal to the correlation length λ of the porosity field. The characteristic volumetric reactivity constant is chosen to be equal to

$$\gamma_0 = \frac{k_p}{\langle m_0\rangle}, \tag{4.7}$$

where $\langle m_0\rangle$ is the average hydraulic radius at the initial time.

Let us now give the major output quantities. At the field scale, one is usually interested in the macroscopic properties of the medium. Several macroscopic quantities were systematically measured. The first one is the average macroscopic porosity $\langle\varepsilon\rangle$,

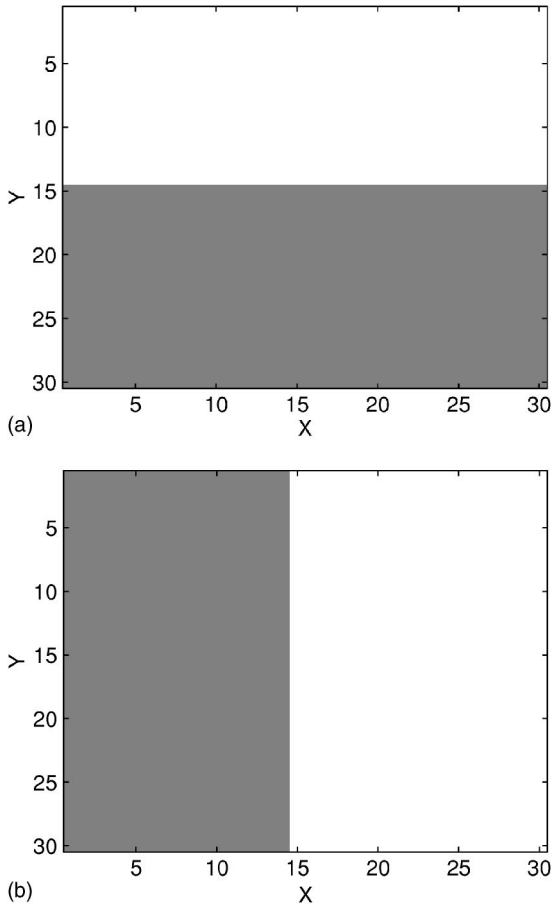

FIG. 3. Porosity of a bilayered porous medium for cases A and B. Flow is parallel to the *x*-axis. The white and grey zones correspond to $\varepsilon_1^0=0.2$ and $\varepsilon_2^0=0.4$, respectively.

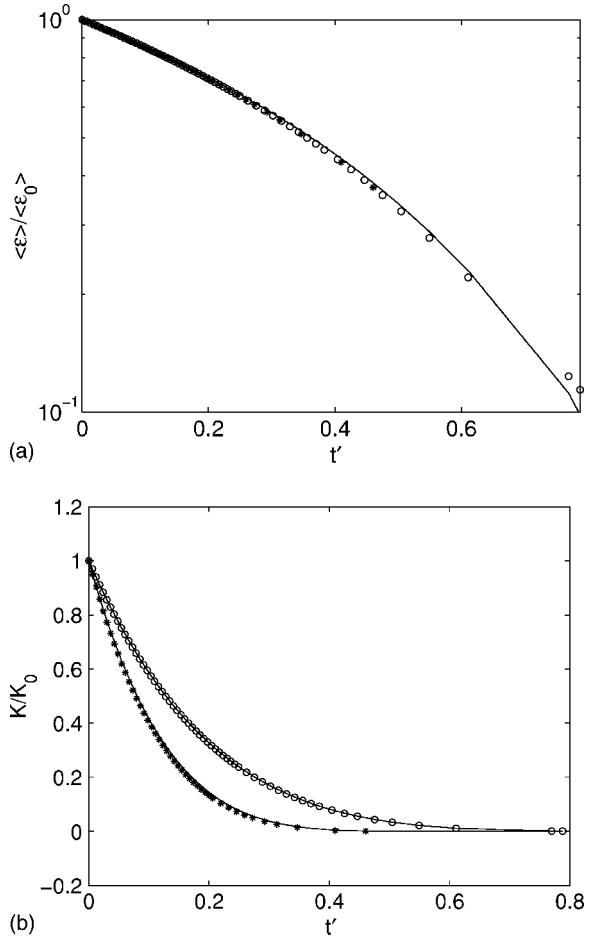

FIG. 4. Numerical results in a bilayered medium for cases A and B denoted by ○ and ∗, respectively. Flow is parallel to the *x*-axis. The solid lines represent the analytical solutions.

$$\frac{\langle \varepsilon \rangle_{t'}}{\langle \varepsilon_0 \rangle} = \frac{\int_{\Omega'} \varepsilon(t') \mathrm{d}^3\mathbf{r}'}{\int_{\Omega'} \varepsilon(t_0') \mathrm{d}^3\mathbf{r}'}, \tag{4.8}$$

where Ω' is the unit cell. The macroscopic permeability is determined by means of the Darcy law

$$\frac{K_t}{K_0} \propto \frac{\overline{V_{t'}'}}{\overline{V_{t_0'}'}}, \tag{4.9}$$

where $\overline{V_{t'}'}$ is the macroscopic seepage velocity at time t'. During the simulations, the macroscopic pressure gradient $\overline{\nabla P}$ is kept constant.

The total amount of deposit per unit volume as a function of time t' is given by

$$Q_{\mathrm{dep}}(t') = \int_{t_0'}^{t'} \frac{1}{\Omega'} \int_{\Omega'} \gamma' \varepsilon C' \mathrm{d}^3\mathbf{r}' \mathrm{d}t'. \tag{4.10}$$

Two autocorrelation functions will be used to characterize the evolution of the porosity field. $R_{\parallel}(\mathbf{u})$ is calculated along the main pressure gradient and $R_{\perp}(\mathbf{v})$ is calculated perpendicular to the main pressure gradient

$$R_{\parallel}(\mathbf{u}) = \frac{\langle [\varepsilon(\mathbf{x}+\mathbf{u}) - \mu_\varepsilon][\varepsilon(\mathbf{x}) - \mu_\varepsilon] \rangle}{\langle [\varepsilon(\mathbf{x}) - \mu_\varepsilon]^2 \rangle}, \tag{4.11a}$$

$$R_{\perp}(\mathbf{v}) = \frac{\langle [\varepsilon(\mathbf{x}+\mathbf{v}) - \mu_\varepsilon][\varepsilon(\mathbf{x}) - \mu_\varepsilon] \rangle}{\langle [\varepsilon(\mathbf{x}) - \mu_\varepsilon]^2 \rangle}, \tag{4.11b}$$

where $\mathbf{u}$ and $\mathbf{v}$ are spatial shifts parallel and perpendicular to $\overline{\nabla P}$, respectively.

It is obviously shown by the previous developments that the dimensionless parameters are numerous, namely, the artificial parameters which are only useful in the course of the numerical calculations, but which do not possess any physical meaning such as the size of the unit cell N_c and the porosity step $\Delta\varepsilon_{\max}$, the basic physical parameter Da, the parameters which characterize the initial porosity distribution.

V. RESULTS AND DISCUSSION

In this work, the evolution of the macroscopic parameters with time is taken into account by means of a quasisteady

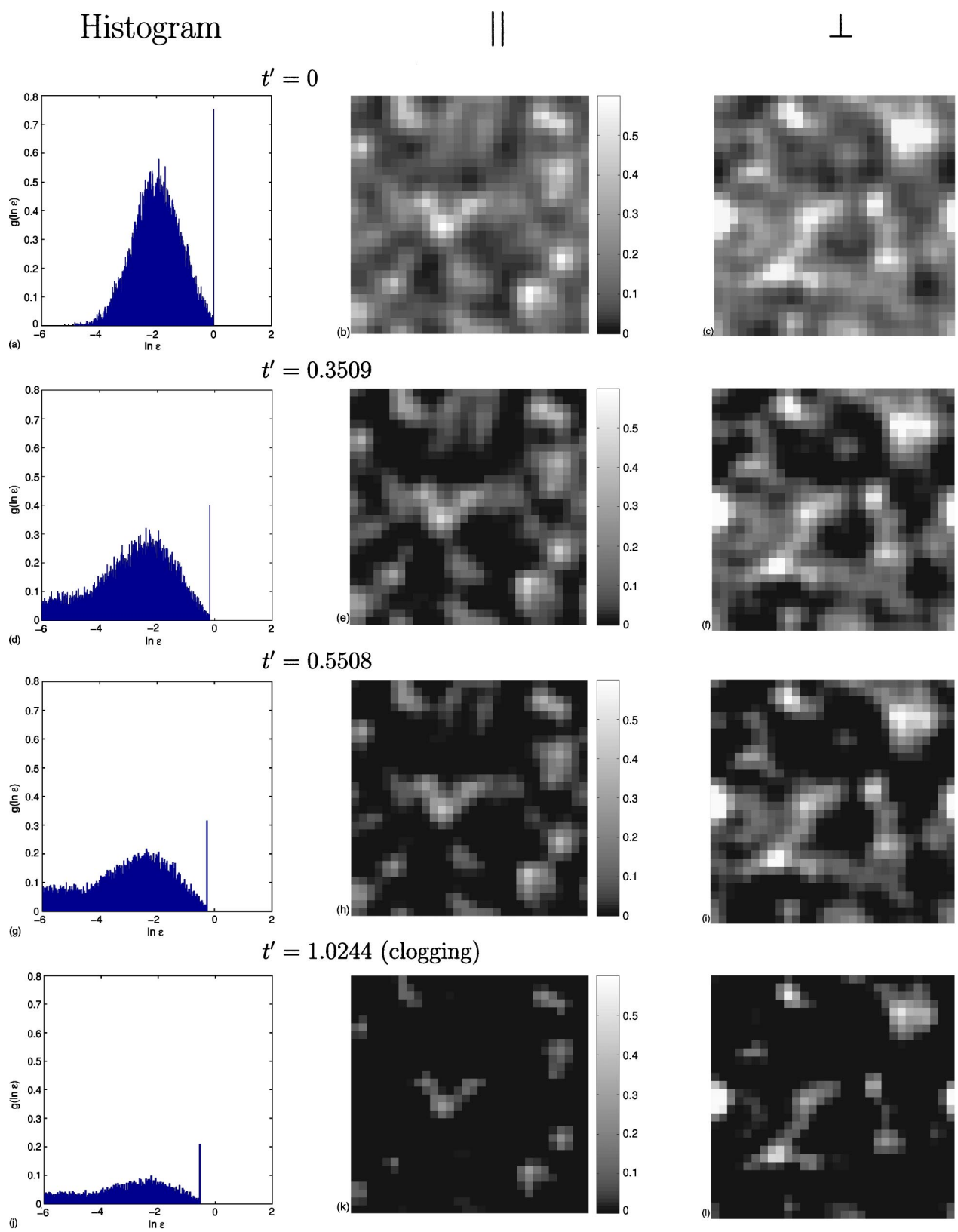

FIG. 5. Evolution of a porous medium with an initial lognormal porosity distribution. Each line corresponds to a different time. The left row is the probability density $g(\ln \varepsilon)$ of $\ln(\varepsilon(\mathbf{r}', \mathbf{t}'))$; the central one is a cross section of the porosity field parallel to the pressure gradient; the right one is perpendicular to the pressure gradient. $\mathrm{Da} = 8 \times 10^{-6}$. The porosity convention is given by the vertical bars.

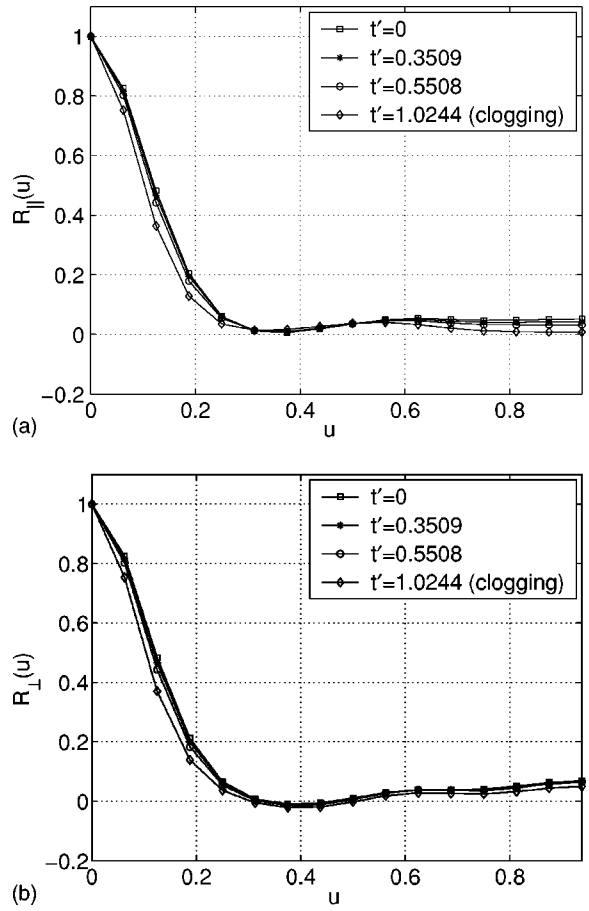

FIG. 6. Evolution of the correlation functions $R_{\parallel}(u)$ (a) and $R_{\perp}(u)$ (b) for the illustrative case. The dimensionless length u is normalized by the half-size of the unit cell. $\mathrm{Da}=8\times10^{-6}$.

approximation. A test presented in the following section is designed to study the influence of the discontinuities introduced into the code due to the steady state approach. Other verifications are done in order to study the effects of the discretization of the porous medium and of the statistical fluctuations on the output results.

A. Preliminaries

1. Simple deterministic media

Consider a two-dimensional porous medium which consists of two homogeneous layers with initial porosities $\varepsilon_1^0=0.2$ and $\varepsilon_2^0=0.4$. We suppose that the macroscopic pressure gradient is imposed along the x direction and is kept constant with time. The layers can be either parallel or perpendicular to the x-axis. These two situations will be referred to as cases A [Fig. 3(a)] and B [Fig. 3(b)], respectively. For both cases, the evolution of the macroscopic parameters can be predicted analytically. In such systems, the liquid concentration C' is expected to be uniform in space. Thus, it is equal to its average value $C'=1$ which is kept constant with time. Then,

$$\varepsilon_i=\left(-\frac{3}{4}\frac{\langle m_0\rangle}{f'}t'+(\varepsilon_i^0)^{3/4}\right)^{4/3},\quad i=1,2, \tag{5.1a}$$

$$\langle\varepsilon_A\rangle=\langle\varepsilon_B\rangle=0.5(\varepsilon_1+\varepsilon_2), \tag{5.1b}$$

where ε_i is the porosity of the ith layer. The calculated mean porosity values are compared with the analytical solutions in Fig. 4(a). For both cases, the numerical results match the analytical curves very satisfactorily. Small differences are only observed at large times when porosity is low. Note that in the calculations, the hydraulic radius was assumed to be constant for low porosity values; this simplification explains the small differences between numerical and analytical results in this case.

For case A, the macroscopic permeability K_A is the sum of the permeabilities of the layers $K_A=K_1+K_2$. For case B, the macroscopic permeability $K_B=(K_1^{-1}+K_2^{-1})^{-1}$. Remind that the permeability of each layer K_i is given by (3.1). Numerically, the macroscopic permeability is obtained by means of the Darcy equation. The calculated values are compared to the analytical solution in Fig. 4(b). The agreement is perfect for both cases.

2. Illustrative case for random media

Statistically homogeneous media are considered as three-dimensional spatially periodic media, composed of identical unit cells of size $L_c=30$ m. The cell is discretized into $N_c^3=30\times30\times30$ elementary cubes. Since the lognormal distribution is the most common for porous media [20], systematic calculations have been performed for log-normally distributed initial porosity fields with a Gaussian correlation function. The initial porosity is supposed to be $\langle\varepsilon_0\rangle=0.2$ with a standard deviation $\sigma_0=0.2$. The correlation length λ is equal to 8 m. Because of the finite size of the unit cell, it is useful to define the ratio λ/L_c which compares the correlation length to the size of the cell. In this case, $\lambda/L_c=8/30$. This particular porous medium is displayed in Fig. 1(a).

The Damköhler number is chosen to be based on the correlation length λ (cf. Sec. IV C). We assumed $\mathrm{Da}=8\times10^{-6}$. The presence of 8 in the Damköhler number is not arbitrary. In fact in numerical simulations, it is more convenient to use the Damköhler number $\mathrm{Da}_{\mathrm{num}}$ based on the size of the elementary cube a. $\mathrm{Da}_{\mathrm{num}}$ is a purely numerical parameter which is used in the course of the numerical calculations since its application provides the dimensionless discretization steps $\Delta\mathbf{r}'$ equal to 1. The corresponding Da is easily obtained from the relation

$$\mathrm{Da}=\mathrm{Da}_{\mathrm{num}}\frac{\lambda}{a}, \tag{5.2}$$

which means that $\mathrm{Da}_{\mathrm{num}}=10^{-6}$ yields $\mathrm{Da}=8\times10^{-6}$.

Before running the code, it is necessary to determine an adequate porosity threshold $\Delta\varepsilon_{\max}$ for the steady state algorithm described in Sec. IV A. Some numerical tests showed that as long as $\Delta\varepsilon_{\max}\leqslant10^{-2}\varepsilon_0$, the various curves collapse onto a single curve. Hence, $\Delta\varepsilon_{\max}$ was chosen equal to $10^{-2}\varepsilon_0$ in the rest of the simulations. The calculations are run as long as the porous medium is sufficiently permeable. As it was mentioned before, we suppose that the porous medium is clogged if its macroscopic permeability is 10^3 times smaller than the initial one.

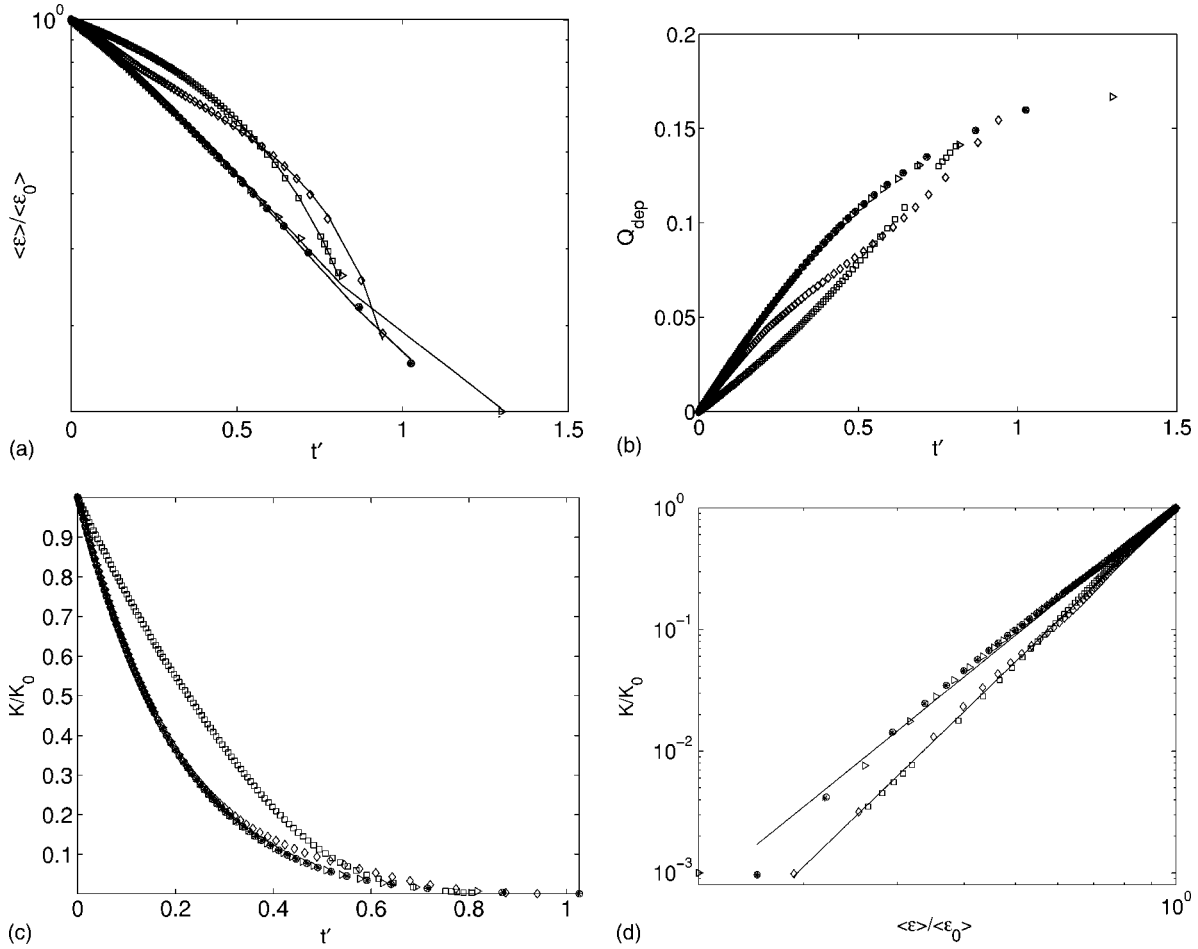

FIG. 7. Macroscopic parameters for various Damköhler numbers for the illustrative case. Data are for $\mathrm{Da}=8\times10^{-6}$ (○), 0.8 (▷), 8×10^{-2} (∗), 8 (◇), and 80 (□). The solid lines represent least-square fits.

The output quantities include the porosity field and the macroscopic parameters as functions of time. Some probability densities and cross sections of the porosity field for successive times are shown in Fig. 5. The left cross section is taken at the center of the domain parallel to $\overline{\nabla P}$ and the right one perpendicular to $\overline{\nabla P}$; in Fig. 5, they are denoted by the subscripts $\parallel$ and $\perp$, respectively. This set of three pictures is plotted for successive times until clogging. These sections show that porosity changes smoothly. It appears that the regions with low porosity are clogged first. At clogging, regions with large porosity still exist.

The probability densities $g(\ln\varepsilon)$ are displayed in Fig. 5. Hence, for the initial lognormally distributed porosity field, $g(\ln\varepsilon)$ is Gaussian. Since lognormally distributed values vary from zero to infinity, values of porosity larger than 1 were truncated; due to this truncation, some elementary cubes have a porosity equal to 1 and they correspond to the vertical bars in Fig. 5. During deposition, the probability density shape gets flat and shifts to the left.

The evolution of the correlation functions is shown in Fig. 6. Deposition only slightly affects the correlation function of the porosity field. This uniform reduction of porosity is expected when the liquid concentration does not vary much. In this case, it is interesting to compare the obtained macroscopic parameters with the elementary solution (cf. Sec. IV B) derived for the situation where the liquid concentration and the hydraulic radius are constant. Note that the variations of the hydraulic radius implemented in the code are small.

The evolution of the mean porosity as a function of time is shown in Fig. 7(a). Since the curve is linear in a semilog plot, the mean porosity is an exponential function of time. The mean square approximation gives

$$\frac{\langle\varepsilon\rangle}{\langle\varepsilon_0\rangle}\approx\exp(-1.72\,t'). \tag{5.3}$$

The calculated mean porosity is quite close to the elementary solution (4.6). Another important macroscopic parameter is the total amount of deposit per unit volume Q_{dep}. Figure 7(b) gives Q_{dep} as a function of mean porosity. A least-square approximation yields

$$Q_{\mathrm{dep}}\approx\langle\varepsilon_0\rangle-\langle\varepsilon\rangle. \tag{5.4}$$

At each time, the total amount of deposited matter is proportional to the change in mean porosity during the corresponding time interval. The evolution of the macroscopic permeability with time and its relation to the mean porosity is a question of particular interest and importance. Figures 7(c) and 7(d) show the macroscopic permeability as a function of time and of the mean porosity, respectively; the variations of

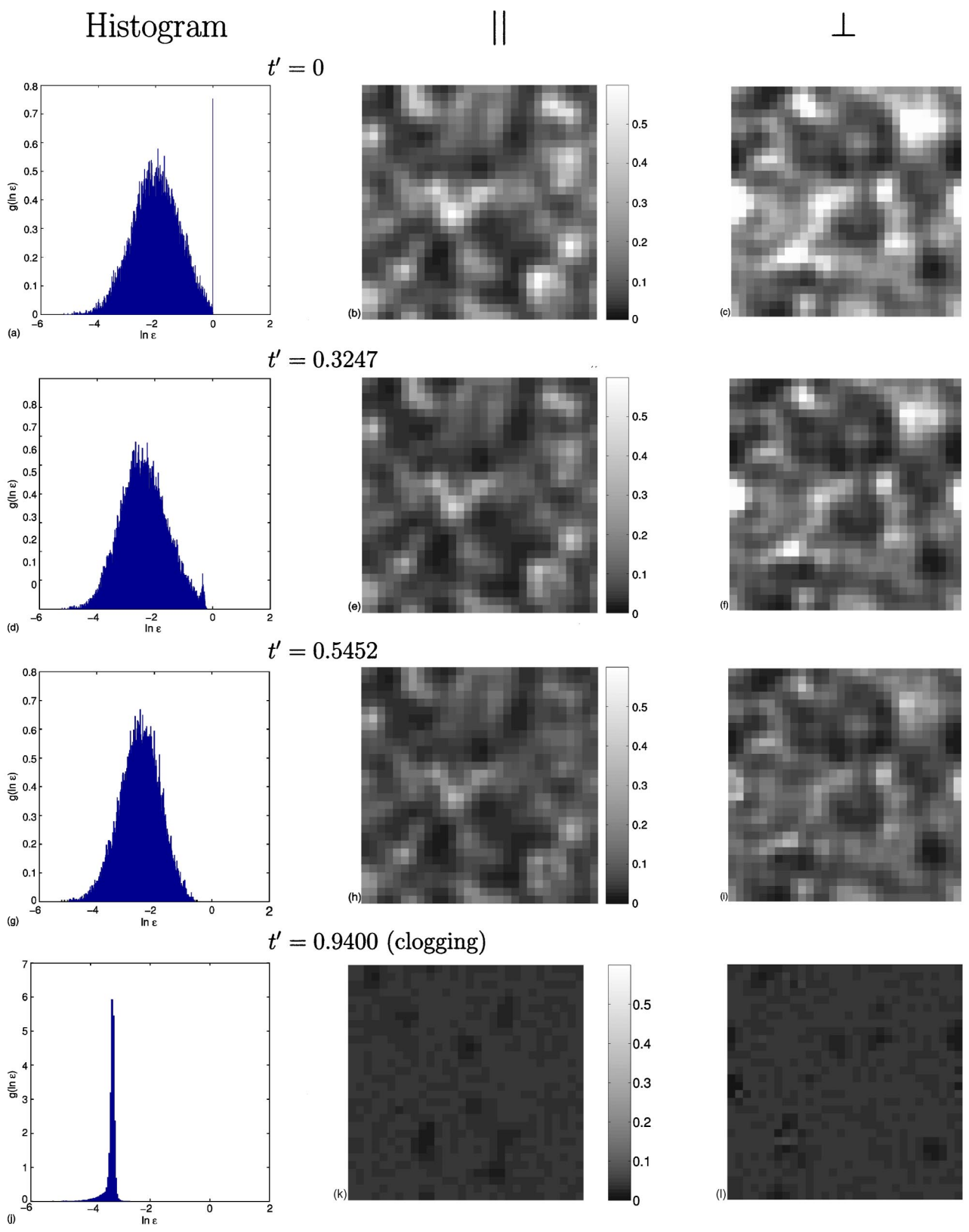

FIG. 8. Evolution of a porous medium with an initial lognormal porosity distribution. Each line corresponds to a different time. The left row is the probability density $g(\ln \varepsilon)$ of $\ln(\varepsilon(\mathbf{r}', \mathbf{t}'))$; the central one is a cross section of the porosity field parallel to the pressure gradient; the right one is perpendicular to the pressure gradient. Da=8. The porosity convention is given by the vertical bars.

TABLE I. General analysis of the data. Values denoted by $*$ correspond to simulations where the clogging condition was not obtained due to numerical difficulties; thus, the time T_c' corresponds to the last calculated one.

						$\frac{\langle\varepsilon\rangle}{\langle\varepsilon_0\rangle}\approx\Sigma_{n=0}^{3}a_n t'^n$						
N	Initial distribution	Da	$\langle\varepsilon_0\rangle$	σ_0	λ/L_c	a_3	a_2	a_1	a_0	$\frac{K}{K_0}\approx\exp\left(\frac{\langle\varepsilon\rangle}{\langle\varepsilon_0\rangle}\right)^{\eta}$, η	T_c'	$Q_{\mathrm{dep}}(T_c')$
1	Lognormal	8×10^{-6}	0.2	0.2	8/30	−0.04	0.66	−1.44	1	3.55	1.02	0.160
2		8×10^{-2}										
3		0.8				−0.11	0.75	−1.47	1	3.41	1.29	0.167
4		8				−0.86	1.27	−1.29	1	4.18	0.94	0.154
5		80				0.12	−0.47	−0.61	1	4.28	0.81*	0.141*
6		8×10^{-6}	0.4	0.2		0.39	0.18	−1.48	1	3.48	0.78	0.338
7			0.2	0.1		0.38	0.19	−1.48	1	3.55	0.78	0.169
8			0.2	0.3		−0.04	0.66	−1.44	1	3.77	1.18	0.146
9		8	0.4	0.2		−0.86	0.99	−1.44	1	4.18	0.70	0.318
10			0.2	0.1		−0.90	0.99	−1.41	1	4.16	0.71	0.160
11			0.2	0.3		−0.86	1.27	−1.30	1	4.00	1.24	0.148
12	Uniform	8×10^{-6}	0.2	0.115	0	0.04	0.47	−1.43	1	3.20	0.91	0.178
13	Gaussian			0.2	8/30	0.04	0.33	−1.22	1	3.58	1.02	0.180
14	Self-affine					−0.05	0.33	−1.22	1	3.35	1.06	0.186
15	Uniform	8	0.2	0.115	0	−0.01	0.53	−1.43	1	3.35	0.75	0.156
16	Gaussian			0.2	8/30	−0.39	0.69	−1.17	1	4.03	0.95	0.174
17	Self-affine					−0.07	0.50	−1.24	1	3.44	0.78	0.151
18	Lognormal	8×10^{-6}	0.2	0.2	8/20	−0.02	0.14	−0.37	1.25	3.50	1.02	0.162
19					8/40	−0.05	0.44	−1.28	1.88	3.80	0.95	0.155
20		8			8/20	−0.18	1.55	−4.00	3.63	4.42	0.93	0.156
22					8/40	0.17	−0.17	−1.21	2.21	4.10	0.65*	0.103*

ε are close to a power law which can be approximated as

$$\frac{K}{K_0}\approx\left(\frac{\langle\varepsilon\rangle}{\langle\varepsilon_0\rangle}\right)^{\eta}, \tag{5.5}$$

with $\eta=3.55$. Note that locally an analogous power-law permeability-porosity relation was used with an exponent equal to 4 [see Eq. (3.1)]. The elementary solution is obtained by applying this relation to the macroscopic permeability as a function of $\langle\varepsilon\rangle$,

$$\frac{K_e}{K_0}\approx\left(\frac{\langle\varepsilon\rangle_e}{\langle\varepsilon_0\rangle}\right)^{4}, \tag{5.6}$$

where the index e denotes the elementary solution. The calculated macroscopic permeability is very close to this elementary solution.

When deposition begins, the porosity decreases according to the elementary solution which is derived for a constant liquid concentration. Then, the rate of the porosity reduction accelerates relatively to the elementary solution.

As mentioned in Sec. II C, the amount of precipitating solute can be limited. Such a limitation would imply that the proposed curves are valid for a time t' smaller than a certain critical time t_c'; for larger times, deposition stops because there is nothing to deposit anymore. For instance, for Da $=0.8$, suppose that Q_{dep} is at most equal to 0.1; Fig. 7(b) implies that $t_c'\approx0.5$. Therefore, for $t'>t_c'$, Q_{dep} is equal to 0.1.

3. Statistical fluctuations

Since the initial configurations are produced at random, one should average over many of them in order to obtain meaningful statistical quantities. However, such an approach is very expensive in terms of computer time. Instead, we provide here an analysis of the output results for different realizations of the initial random porosity field.

In addition to the illustrative case, two groups of calculations were done for the same set of parameters. The porosity field is lognormal; the mean porosity $\langle\varepsilon_0\rangle$ is equal to 0.2, the standard deviation σ_0 to 0.2 and the ratio λ/L_c is equal to 8/30. The calculations were done for Da $=8\times10^{-6}$ and Da $=8$. The agreement between the realizations is very good for both regimes, except may be in the period close to clogging. Therefore, the calculated macroscopic quantities are not significantly influenced by the statistical fluctuations. Thus, the tedious averaging procedure described above seems to be useless.

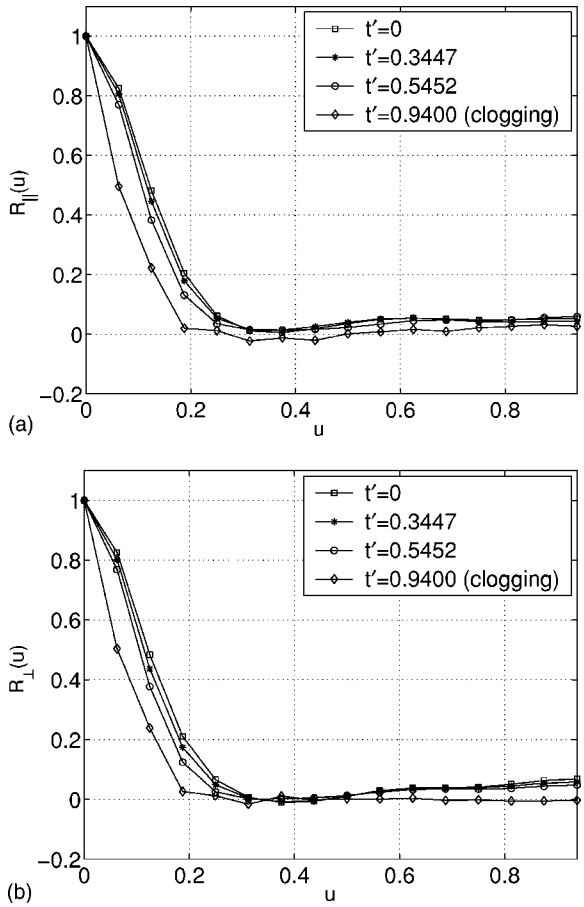

FIG. 9. Evolution of the correlation functions $R_{\|}(u)$ (a) and $R_{\perp}(u)$ (b). The dimensionless length u is normalized by the half-size of the unit cell. Da=8.

4. The influence of the size of the unit cell

The size L_c of the unit cell is one of the artificial parameters introduced in the simulations. For correlated media, it is usually supposed that L_c is large enough so that the unit cell can contain many "independent" samples of the porous medium. If this condition is not satisfied, the discrete model fails to represent the random character of a real medium. Thus, it is likely that an improper choice of the cell size can cause significant errors in the estimation of the macroscopic parameters of the random medium. The ratio λ/L_c was used to characterize the cell size. In the illustrative case, λ/L_c is equal to $8/30$. Two more calculations were done for λ/L_c equal to $8/20$ and $8/40$.

For all cases, the mean porosity value $\langle\varepsilon\rangle$ is equal to 0.2 and the standard deviation $\sigma_0=0.2$. For all calculations, we kept the ratio λ/a constant and equal to 8 as for the illustrative case. In order to change the ratio λ/L_c the size of the unit cell was varied. The mean porosity value and the total amount of deposit were shown not to be influenced by λ/L_c. On the contrary, the macroscopic permeability is a bit sensitive to the variations of λ/L_c especially for small Damköhler numbers. Note that correct results are only obtained for sufficiently large unit cells, but the computational time increases significantly with the increase of the domain size. The presented tests have shown that the ratio $\lambda/L_c=8/30$ would be an optimal choice.

5. Influence of the discretization

It should be reminded that the porosity field is discretized. In principle, the size of the elementary cubes should be very small compared to the correlation length λ in the practically important case of correlated media. The test included three calculations for porous media discretized into 120×120, 60×60, and 30×30 elementary cubes. In all three cases, the porosity field is lognormally distributed with $\langle\varepsilon\rangle=0.4$, $\sigma=0.2$, and $\lambda/L_c=8/30$. The calculations were performed for $\mathrm{Da}=32\times10^{-6}$ and $\mathrm{Da}=32$.

For small Damköhler number, the results are not influenced by the discretization. For large Damköhler number, only the macroscopic permeability for $N_c=120$ is slightly different at the beginning of the deposition. Thus, discretization is shown to play a very small role.

B. Influence of the Damköhler number

As it was mentioned before, the basic physical parameter is the Damköhler number which compares the reaction rate to convection. For the small Damköhler number equal to 8×10^{-6} considered in the illustrative case, convection is very large compared to reaction. As it was shown in this case, deposition causes smooth changes to the porosity field. The evolution of the mean porosity can be predicted by the elementary solution derived for a situation where the concentration C' and the reactivity γ' are constant. Another behavior is expected when the Damköhler number is high. The domination of reaction over convection can cause significant variations of the concentration field and affect the macroscopic properties. In order to investigate the role of the Damköhler number, calculations were done for $\mathrm{Da}=8\times10^{-2}$, 0.8, 8, and 80. The initial porosity field corresponds to the one used in the illustrative case. Note that the Damköhler number is based on initial quantities such as the macroscopic velocity V^* and the reactivity γ_0. Both will vary during deposition and the actual Damköhler number will increase.

The macroscopic parameters for the various Da are compared to the illustrative case in Fig. 7. The curves for $\mathrm{Da}=8\times10^{-2}$ collapse onto the curves of the illustrative case where $\mathrm{Da}=8\times10^{-6}$ [Fig. 7(a)]. On the contrary, for Da=8 and 80, the behavior of the mean porosity differs considerably from the illustrative case. The mean porosity curve is not exponential anymore. At the beginning of deposition, the mean porosity diminishes more slowly than for the illustrative case and after a certain time it decreases sharply. Clogging occurs earlier than for the illustrative case. For Da =0.8, the mean porosity values match well the results for the illustrative case except for the times close to clogging. Clogging occurs a bit later than for the illustrative case.

The mean porosity evolution can be approximated by a polynomial of degree 3 in all cases (Table I). The evolution of the total amount of deposit per unit volume is proportional to the mean porosity change. Q_{dep} is shown as a function of time in Fig. 7(b). Finally, at clogging, the total amount of

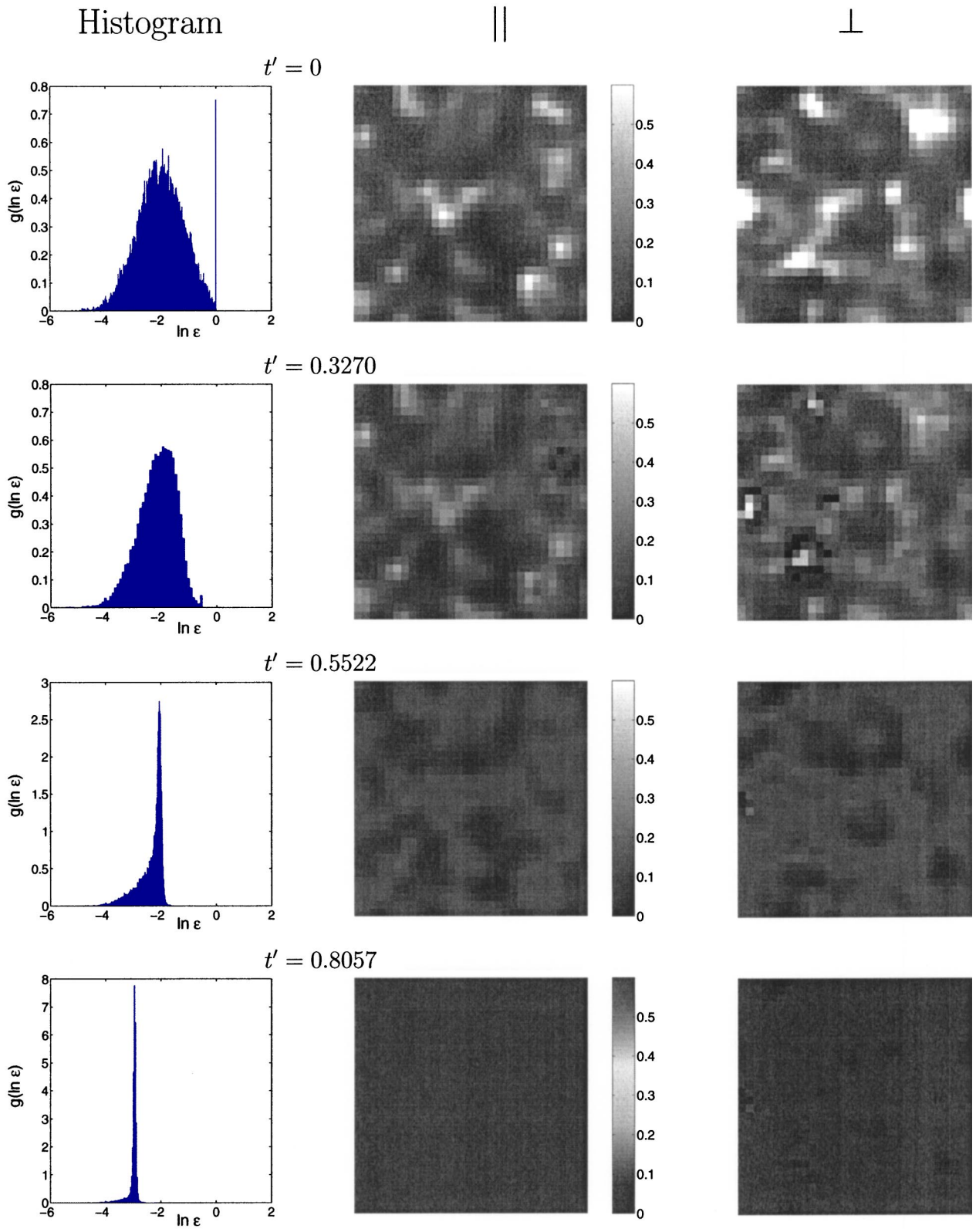

FIG. 10. Evolution of a porous medium with an initial lognormal porosity distribution. Each line corresponds to a different time. The left row is the probability density $g(\ln \varepsilon)$ of $\ln(\varepsilon(\mathbf{r}', \mathbf{t}'))$; the central one is a cross section of the porosity field parallel to the pressure gradient; the right one is perpendicular to the pressure gradient. Da=80. The porosity convention is given by the vertical bars.

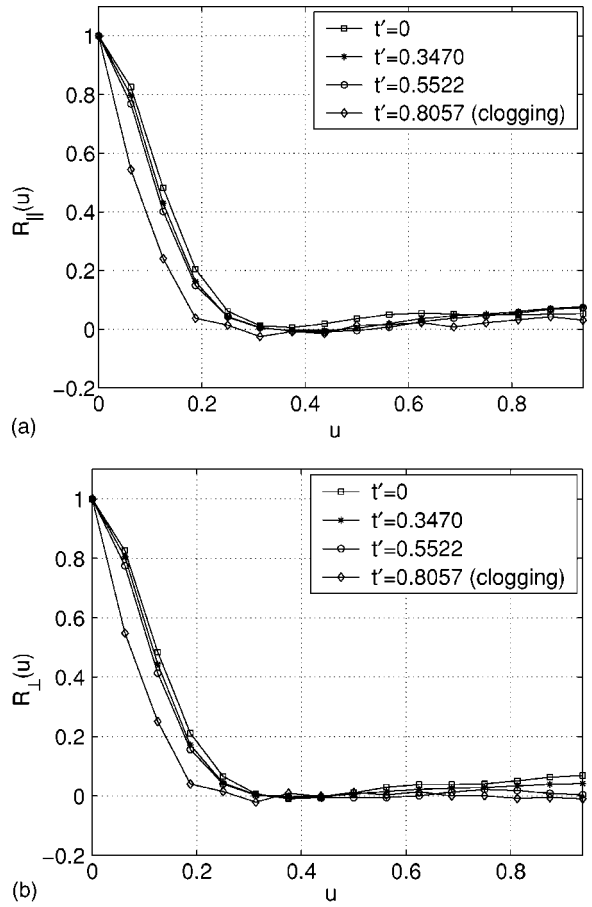

FIG. 11. Evolution of the correlation functions $R_{\|}(u)$ (a) and $R_{\perp}(u)$ (b). The dimensionless length u is normalized by the half-size of the unit cell. Da=80.

deposit per unit volume is nearly the same for all cases. The macroscopic permeability as a function of the dimensionless time is shown in Fig. 7(c), the results for $\mathrm{Da}=8\times10^{-6}$, 8×10^{-2}, 0.8 and 8 are close to each other; only Da=80 differs considerably from the others. Thus, it is remarkable that the macroscopic permeabilities for Da=8 and Da=80 collapse onto a single curve as a function of the mean porosity. For all cases, K is a power of $\langle\varepsilon\rangle$ with an exponent $\eta_s=3.55$ for small Damköhler numbers ($\mathrm{Da}=8\times10^{-6}$ and 8×10^{-2}) and $\eta_h=4.22$ for high Damköhler numbers (Da=8 and 80).

Thus, two different regimes are observed for small and large Damköhler numbers. The evolution of the porosity field for high Da can be observed in Fig. 8 for Da=8 and in Fig. 9 for Da=80. Contrarily to small Da, a large proportion of matter is deposited in the regions where porosity is high. This modifies the correlations displayed in Fig. 10 for Da =8 and in Fig. 11 for Da=80. At clogging, the porosity field is nearly uniform.

The case where Da=0.8 is different from the rest of the results. At the beginning of deposition, the evolution of the porosity field is analogous to the illustrative case where Da is small. The porosity field sections and the probability densities are displayed in Fig. 12. The evolution of the correlation functions is shown in Fig. 13. At clogging, the porosity field is not uniform as for large Damköhler numbers, but the probability density $g(\ln\varepsilon)$ is less spread than for small Damköhler numbers. There are no regions with high porosity. Thus, the situations where $\mathrm{Da}\approx1$ can be considered as intermediate between the regime where convection is dominant $\mathrm{Da}<1$ and the regime where reaction is dominant $\mathrm{Da}>1$.

It is necessary to add that the clogging time T_c' has no particular importance since clogging has been somewhat arbitrarily defined. Hence, attention should be focused on the evolution of the macroscopic parameters with time.

In the following, each calculation will be done for a small and a large Damköhler number, since the system is expected to behave differently in these conditions. More precisely, we mean the evolution of the probability density $g(\ln\varepsilon)$ and the relation between the macroscopic permeability and the mean porosity. As for the mean porosity evolution, it will be shown later that the exponential decrease for small Damköhler numbers only occurs for lognormally distributed porosity fields. Polynomial approximations of the mean porosity values provide a very good fit for all the results described in this work. Note that they are only valid for times $t'\in[0,T_c']$. The data are gathered in Table I.

C. Influence of the parameters characterizing the initial porosity distribution

This section studies the influence of the mean $\langle\varepsilon_0\rangle$ and of the standard deviation σ_0 of the initial porosity field on the evolution of the macroscopic parameters during deposition. The initial porosity field is assumed to be lognormally distributed. The ratio λ/L_c is equal to $8/30$.

The first test addresses the effect of the mean porosity value. $\langle\varepsilon_0\rangle$ is taken to be equal to 0.4 and $\sigma_0=0.2$. The second and third calculations are done for $\langle\varepsilon_0\rangle=0.2$ and σ_0 equal to 0.1 and 0.3. The calculations were performed for $\mathrm{Da}=8\times10^{-6}$ (Fig. 14) and Da=8. The calculated mean porosity values are compared to the analytical solution derived for a homogeneous medium. As it can be seen, for situations where the ratio $\sigma_0/\langle\varepsilon_0\rangle$ is small, the mean porosity is close to the analytical solution for a homogeneous medium. Note that the mean porosity decreases faster for the homogeneous medium than for the heterogeneous ones. The clogging time increases with $\sigma_0/\langle\varepsilon_0\rangle$. Moreover, it is obvious now that the exponential decrease of the mean porosity value takes place only for heterogeneous systems with $\sigma_0/\langle\varepsilon_0\rangle$ sufficiently large.

The amount of deposit necessary to clog the medium is higher for smaller σ_0, but the variations are not significant. The initial porosity value strongly affects Q_{dep} [Fig. 14(b)]. The higher the initial mean porosity, the larger the deposit amount necessary to clog the medium.

The macroscopic permeability as a function of the mean porosity does not depend on the average statistical properties of the initial field. The results collapse onto a single curve for both Damköhler numbers [Fig. 14(d)]. The macroscopic permeability evolutions are different, because of different mean porosity values.

D. Uniform, Gaussian, and self-affine porosity distributions

The random porosity field is characterized by the porosity probability density and the spatial organization of the porous

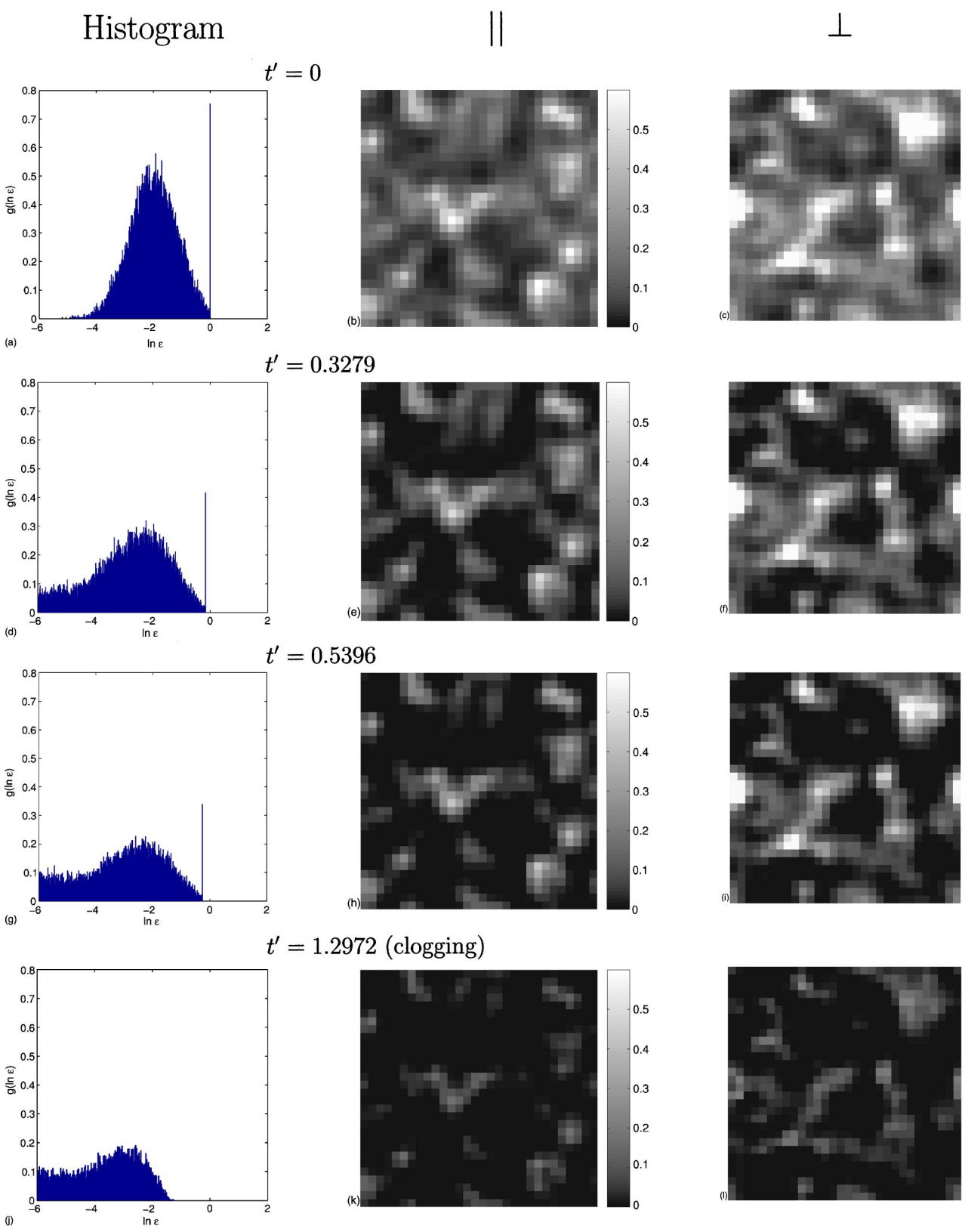

FIG. 12. Evolution of a porous medium with an initial lognormal porosity distribution. Each line corresponds to a different time. The left row is the probability density $g(\ln \varepsilon)$ of $\ln(\varepsilon(\mathbf{r}', \mathbf{t}'))$; the central one is a cross section of the porosity field parallel to the pressure gradient; the right one is perpendicular to the pressure gradient. Da=0.8. The porosity convention is given by the vertical bars.

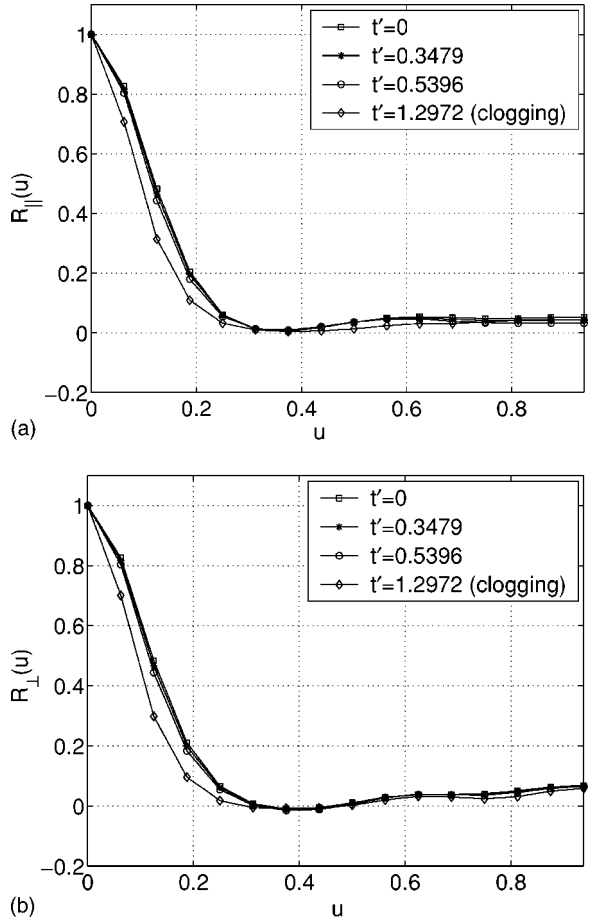

FIG. 13. Evolution of the correlation functions $R_{\parallel}(u)$ (a) and $R_{\perp}(u)$ (b). The dimensionless length u is normalized by the half-size of the unit cell. Da=0.8.

material; this latter aspect can be described by correlation functions such as (3.18). Four different porosity fields were used in this study, namely Gaussian, lognormal, self-affine, and uniform. The detailed description is given in Sec. III B. Gaussian and lognormal fields are characterized by the same Gaussian correlation function; they are useful to study the influence of the porosity variability on the output results. On the other hand, Gaussian and self-affine fields have the same Gaussian distribution of the porosity values, but their spatial organization is very different due to different correlation functions. By comparing these two cases, one can estimate the influence of the spatial correlation on the results.

All the correlated fields are generated with $\langle\varepsilon_0\rangle=0.2$ and $\sigma_0=0.2$. For the self-affine distribution, H was taken equal to 2. The uniform distribution corresponds to porosities uniformly distributed over the interval [0,0.4]. The uniform distribution is distinct from the others since it is not correlated and since σ_0 is determined by the interval of variations; here $\sigma_0^u \approx 0.115$.

The porosity fields are shown in Fig. 1 and their aspects are seen to be very different. In the uniformly distributed porous medium, porosity changes abruptly because of its uncorrelated character. The Gaussian porosity field is characterized by smooth porosity changes, and regions with high porosity and low porosity are clearly distinguishable. The aspect of the lognormal porosity field is similar to the Gaussian one, but the variations are more pronounced, i.e., the porosity is either very small or very high. The self-affine porosity field displays a more complex spatial structure since both sharp and smooth changes occur around a single elementary cube.

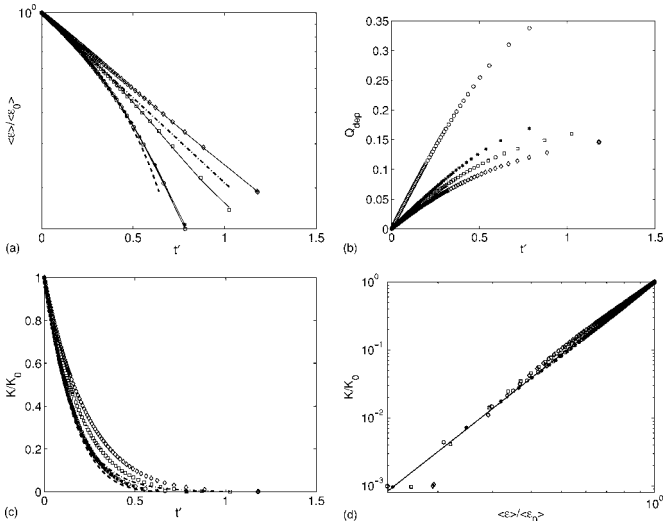

FIG. 14. Influence of the mean initial porosity and of its standard deviation on the macroscopic properties. Data are for $\langle\varepsilon_0\rangle=0.4$ and $\sigma_0=0.2(\bigcirc)$, $\langle\varepsilon_0\rangle=0.2$, $\sigma_0=0.1(*)$, $\langle\varepsilon_0\rangle=0.2$, $\sigma_0=0.3(\diamond)$, illustrative case ($\square$). The solid line represents a least-square data fit. The elementary solution (4.6) is shown by the dashed-dotted lines. The dashed line corresponds to the analytical solution for a homogeneous medium with $\varepsilon=0.2$. $\lambda/L_c=8/30$. Da $=8\times10^{-6}$.

The macroscopic parameters derived for these initial fields are shown in Figs. 15 and 16. As expected, the case of the uniformly distributed porosity field is distinct from the others. For both Damköhler numbers, the mean porosity value decreases faster than for the other cases. For small Damköhler numbers, results for Gaussian and self-affine fields collapse onto a single curve. For large Damköhler numbers, they are close to each other, yet different. Remarkably, the exponential decrease of the mean porosity for small Damköhler numbers is only valid for the lognormal distribution. For the other distributions, the variations can be approximated by a polynomial of degree 3. The least-square approximation coefficients are given in Table I.

The evolution of the mean porosity depends much on the spatial correlation of the porosity field as well as on the variability of the porosity values. At the beginning of deposition, the total amount of deposit per unit volume as a function of time is nearly the same for all the cases. Close to clogging, the results for the lognormal porosity field differ from the others with less deposited matter.

For all Damköhler numbers, the macroscopic permeabilities are of the form (5.5). For small Da, the curves of the macroscopic permeability as a function of the mean porosity are very close to each other for all cases. They are slightly different only for times close to clogging.

For large Da, the relationship between the macroscopic permeability and the mean porosity depends on the spatial

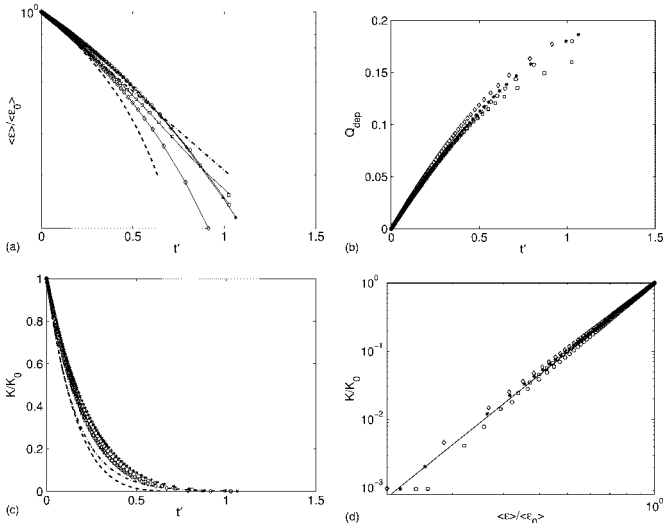

FIG. 15. Evolution of the macroscopic parameters for differently distributed porosity fields. Data are for Gaussian porosity distribution (○), self-affine (∗), uniform porosity (◇), lognormal distribution (□). The solid line represents a least-square data fit. The elementary solution (4.6) is shown by the dashed-dotted lines. The dashed line corresponds to the analytical solution for a homogeneous medium with $\varepsilon=0.2$. $\lambda/L_c=8/30$. $\mathrm{Da}=8\times10^{-6}$.

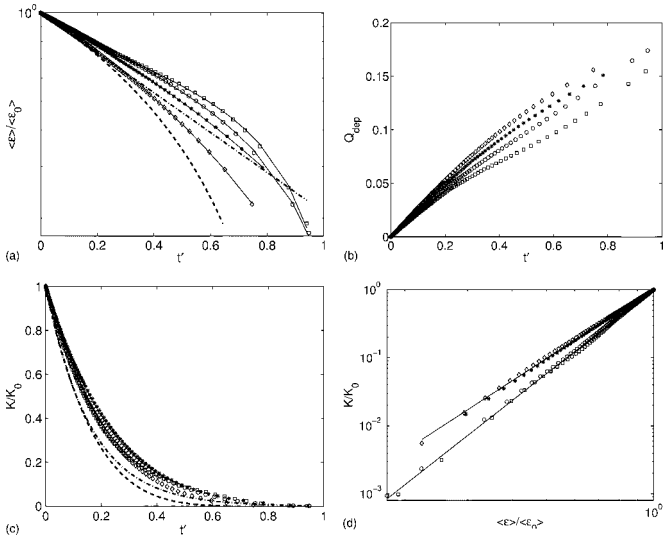

FIG. 16. Evolution of the macroscopic parameters for differently distributed porosity fields. Data are for Gaussian porosity distribution (○), self-affine (∗), uniform porosity (◇), lognormal distribution (□). The solid line represents a least-square data fit. The elementary solution (4.6) is shown by the dashed-dotted lines. The dashed line corresponds to the analytical solution for a homogeneous medium with $\varepsilon=0.2$. $\lambda/L_c=8/30$. $\mathrm{Da}=8$.

organization of the porous medium. For Gaussian and lognormal porosity fields, the curves of the macroscopic permeability as a function of the mean porosity are very close to each other. Note that these porosity fields have the same Gaussian correlation function (3.18). On the other hand, the corresponding results for the self-affine porosity field are very close to those for the uniformly distributed porosity field.

VI. CONCLUDING REMARKS

Deposition in statistically homogeneous media and the subsequent clogging have been studied. A numerical code has been developed which simulates the fluid flow, the transport of a reactive solute in heterogeneous porous media as well as the alterations of the macroscopic properties of the porous medium due to the deposition of the solute onto the pore walls. The code has been tested on several situations where the analytical solution is known and a good agreement was usually observed. Statistically homogeneous media were approximated by spatially periodic media. Since these models are discrete, it is always necessary to validate the choice of several unphysical parameters such as the size of the unit cell or the space discretization step, etc., applied in the simulations. Appropriate tests have been performed. The results have shown that the parameter set was chosen correctly.

The code was systematically applied to predict the evolution of the macroscopic properties of the porous medium during the deposition of a chemically reactive solute. Some important features were revealed by this study. Starting from the same porous medium, one obtains different evolutions of the porous medium properties depending on the Damköhler number which compares the effects of reaction and convection. When convection is dominant ($\mathrm{Da}<1$), the porous medium properties change smoothly. At clogging, the porosity field is analogous to the initial one. The regions where porosity is high, still exist. When reaction is dominant ($\mathrm{Da}>1$), the porous medium is nearly uniform at clogging. For Damköhler numbers close to 1, the evolution of the porous medium is similar to the case $\mathrm{Da}<1$ at the beginning of deposition, and similar to the case $\mathrm{Da}>1$ for the times close to clogging.

The heterogeneity of the medium was observed to have a strong influence on the evolution of the mean parameters. The evolution of the mean porosity value depends on the statistical characteristics of the initial porosity field while the macroscopic permeability as a function of the mean porosity was found to depend mostly on the spatial organization of the porous material.

This study is a first step towards the understanding of deposition phenomena on the macroscopic scale. It would be interesting to extend this work to other cases, particularly to nonuniform local deposition and different constitutive relationships.

ACKNOWLEDGMENTS

Most computations were performed at CINES (Montpellier), subsidized by the MENESR, whose support is gratefully acknowledged. This work was partly supported by the European grant Arisston ENK6-CT-2000-00052.

[1] T. Xu, J. A. Apps, and K. Pruess, J. Geophys. Res. **108**(B2), 2071 (2003).
[2] K. P. Saripalli, P. D. Meyer, D. H. Bacon, and V. L. Freedman, Crit. Rev. Envir. Control, CRC **31**, 311 (2001).
[3] M. Sahimi, G. R. Gavalas, and T. T. Tsotsis, Chem. Eng. Sci. **45**, 1443 (1990).
[4] M. Shapiro and M. Brenner, Chem. Eng. Sci. **43**, 551 (1988).
[5] J. Sallés, J. F. Thovert, and P. M. Adler, Chem. Eng. Sci. **48**, 2839 (1993).
[6] G. P. Matthews, C. J. Ridgway, and J. S. Small, Mar. Pet. Geol. **13**, 581 (1996).
[7] V. V. Mourzenko, J. F. Thovert, and P. M. Adler, Chem. Eng. Sci. **43**, 551 (1996).
[8] S. Bekri, J. F. Thovert, and P. M. Adler, Eng. Geol. (Amsterdam) **48**, 283 (1997).
[9] F. F. Chang and F. Civan, J. Pet. Sci. Eng. **17**, 123 (1997).
[10] T. Xu and K. Pruess, "Coupled modeling of non-isothermal multiphase flow, solute transport and reactive chemistry in porous and fractured media, 1, Model development and validation," Lawrence Berkeley Natl. Lab. Rep. LBNL-42050, pp. 38, Berkeley, California, 1998.
[11] X. Liu, A. Ormond, K. Bartko, Y. Li, and P. Ortoleva, J. Pet. Sci. Eng. **17**, 181 (1997).
[12] Y. Le Gallo, O. Bildstein, and E. Brosse, J. Hydrol. **209**, 366 (1998).
[13] P. M. Adler, *Porous Media. Geometry and Transports* (Butterworth-Heinemann, Washington, DC, 1992).
[14] E. E. Petersen, *Chemical Reaction Analysis* (Prentice-Hall, Englewood Cliffs, N J, 1965).
[15] C. G. Jacquin, Rev. Inst. Fr. Pet. Ann. Combust. Liq. **19**, 921 (1964).
[16] D. Guillot, Ph.D. thesis, ENSM, Paris, 1982.
[17] D. Coelho, J. F. Thovert, and P. M. Adler, Phys. Rev. E **55**, 1959 (1997).
[18] P. M. Adler and J. F. Thovert, *Fractures and Fractures Networks* (Kluwer-Academic, Berlin, 1992).
[19] P. K. Sweby, Lect. Appl. Math. **22**, 289 (1985).
[20] G. Dagan, *Flow and Transport in Porous Formations* (Springer-Verlag, Berlin, New York, 1989).